The Versatile Integrator of Surface and Atmosphere processes Part 1. Model description

Zong-Liang Yang*, Guo-Yue Niu

Department of Geological Sciences, The University of Texas at Austin, Austin, TX 78712-1101, USA

Abstract

This paper describes an integration of recent new developments in snow, runoff and vegetation growth into the National Center for Atmospheric Research Land Surface Model (NCAR LSM). The new model, referred to as the Versatile Integrator of Surface and Atmosphere processes (VISA), has been validated with observed data. The results have demonstrated that the NCAR LSM, after integrating with these new developments, produces improved simulations of snow and runoff over the baseline version, and has an added capability to simulate the dynamics of leaf area index (LAI). Moreover, VISA, through its integration of new schemes, is not only important for studying land–atmosphere interactions in its own right, but also useful for helping interpret results from a parallel modeling activity—the Community Land Model (CLM) project.
© 2003 Elsevier Science B.V. All rights reserved.

Keywords: VISA; Snow; Runoff

1. Introduction

During the past decade, much progress has been made in representing processes of snow (Loth et al., 1993; Lynch-Stieglitz, 1994; Dai and Zeng, 1997; Sun et al., 1999), runoff (Famiglietti et al., 1992; Stieglitz et al., 1997; Chen and Kumar, 2001), and vegetation growth (Foley et al., 1998; Dickinson et al., 1998) in land-surface parameterization schemes. However, a great deal of attention has been focused on one component within one land-surface parameterization scheme at a time. If each of these individual process-based representations is robust, all should be incorporated into a widely used, state-of-the-art land-surface parameterization scheme, and the performance should be evaluated with observations. Such integration and evaluation are critical for understanding, modeling and predicting interactions between land and the atmosphere.

This paper describes an integration of the above new developments in snow, runoff, and vegetation growth into a land surface model (LSM) developed at the National Center for Atmospheric Research (NCAR). Four factors have been considered in selecting the NCAR LSM (Bonan, 1996a) as the baseline model. First, the NCAR LSM is the standard land module in the NCAR Community Climate Model Version 3 (CCM3) (Kiehl et al., 1998) whose code is publicly accessible and widely used. Second, the

---
* Corresponding author. Tel.: +1-512-471-3824; fax: +1-512-471-9425.

E-mail address: liang@mail.utexas.edu (Z.-L. Yang).

NCAR LSM has been well documented (Bonan, 1995a,b, 1996a,b; Bonan et al., 1997; Bonan and Stillwell-Soller, 1998). Third, the treatment of snow and runoff in the NCAR LSM is so simple that further improvements are warranted. Although the carbon dioxide exchange between land and the atmosphere is modeled, its leaf area index is prescribed. Fourth, the NCAR LSM is also used as one of baseline models for constructing the Community Land Model (CLM) (Dai et al., 2003), and hence the results described in this paper will help explain the results in Dai et al. (2003), Zeng et al. (2002) and Bonan et al. (2002).

The NCAR LSM, after integrating with a physically based multilayer snow model, a topography-based runoff scheme and new soil moisture computation scheme, and a vegetation growth scheme, will be referred to as the Versatile Integrator of Surface and Atmosphere processes (VISA). Niu and Yang (2003b-this issue), hereafter referred to as paper 2, describe three different schemes of topography-related runoff in VISA and assess the schemes' sensitivities to key parameters.

2. Implementing a multilayer snow model into the NCAR LSM

2.1. Snow scheme in the NCAR LSM

The NCAR LSM has a bulk layer for snow mass and a blended snow and surface soil layer for the ground surface temperature. The ground heat flux depends on the difference between the skin temperature and the top soil layer temperature, the thickness of the top soil layer, and the snow thickness, which is limited to 1 m. This framework results in underestimates in the simulated snow water equivalent (SWE) (Yang and Niu, 2000).

2.2. A new multilayer snow model

Following Loth et al. (1993), Lynch-Stieglitz (1994), Dai and Zeng (1997), and Sun et al. (1999), a new multilayer physically based snow scheme is developed for use in the NCAR LSM. While a detailed description of the scheme is given in Niu and Yang (2003a), the model is described briefly as follows.

2.2.1. Layer structure

The model has zero to three layers depending on snow depth. While the minimum value is 0.025 m for all layers, the maximum layer thickness is defined as follows:

$$\Delta z_{sno}^1 = 0.05$$

$$\Delta z_{sno}^2 = 0.18$$

$$\Delta z_{sno}^3 = h_{sno} - \Delta z_{sno}^1 - \Delta z_{sno}^2 \qquad (1)$$

where h_{sno} is the total snow depth in meters. If the first layer snow depth exceeds its maximum value, the second layer is created, with energy and water being conserved. If the second layer thickness is less than its minimum value, it will be combined with its neighboring layer with energy and water being conserved.

2.2.2. Snow surface temperature

The snow surface temperature T_g is obtained by iteratively solving the snow surface energy balance equation

$$- S_g + L_g + H_g + \lambda E_g + G$$
$$+ \left(\frac{\partial L_g}{\partial T_g} + \frac{\partial H_g}{\partial T_g} + \frac{\partial \lambda E_g}{\partial T_g} + \frac{\partial G}{\partial T_g} \right) \Delta T_g = 0 \qquad (2)$$

where $\Delta T_g = T_g^{N+1} - T_g^N$ and the superscript N indicates the iteration. S_g, L_g, H_g, λE_g, and G are the net solar radiation, long-wave radiation, sensible heat, latent heat and ground heat fluxes, respectively. The ground heat flux G (positive into the first layer snow) is

$$G = \frac{k_{sno}^1}{\Delta z_{sno}^1} (T_g - T_{sno}^1) \qquad (3)$$

where k_{sno}^1, Δz_{sno}^1 and T_{sno}^1, respectively, are the thermal conductivity, the thickness, and the temperature of the first snow layer. Note that in the above equation, a thinner first layer (Δz_{sno}^1) replaces the total snow depth plus half of the first soil layer ($h_{sno} + \Delta z_{soi}^1/2$) in the

baseline NCAR LSM in order to compute the ground heat flux more accurately.

2.2.3. Subsurface temperatures

The snow temperature T_{sno} for the subsurface layers is expressed as

$$C_{sno} \frac{\partial T_{sno}}{\partial t} = \frac{\partial}{\partial z}\left(k_{sno}\frac{\partial T_{sno}}{\partial z}\right) + S \tag{4}$$

where C_{sno} is the heat capacity, k_{sno} is the effective thermal conductivity, respectively, and S refers to the source or sink term such as the solar radiation, the latent heat from phase change, and the heat from rain. The heat from rain is added on the first layer only. The heat capacity for a volume of snowpack is expressed as

$$C_{sno} = (c_{ice}\theta_{ice} + c_{liq}\theta_{liq}) \tag{5}$$

where c_{ice} and c_{liq} are the volumetric heat capacity of ice and liquid water with values of 2.904×10^6 and 4.188×10^6 (J m^{-3} K^{-1}), respectively. θ_{ice} and θ_{liq} are the partial volumes (m^3 m^{-3}) of ice and liquid water content, respectively. The effective thermal conductivity of snow k_{sno} is the combination of snow thermal conductivity k_s and the conductivity due to vapor diffusion k_v

$$k_{sno} = k_s + k_v \tag{6}$$

The snow thermal conductivity k_s is estimated following Jordan (1991) as

$$k_s = k_{air} + (7.75 \times 10^{-5}\rho_{sno} + 1.105 \times 10^{-5} \times \rho_{sno}^2) \\ \times (k_{ice} - k_{air}) \tag{7}$$

In the relationship, the conductivities of air and ice are 0.023 and 2.29 W K^{-1} m^{-1}, respectively. The thermal conductivity due to vapor diffusion k_v is taken as a function of snow temperature following Anderson (1976).

The source term in Eq. (4) includes the penetration of solar radiation S_{rad}, heat from phase change H_m, which will be described in Section 2.2.5, and the sensible heat from rain H_{rain}

$$S = S_{rad} + H_m + H_{rain} \tag{8}$$

where S_{rad} is the net solar radiation transmission through snow

$$S_{rad} = S_g \exp(-\kappa z) \tag{9}$$

where κ is the attenuation coefficient as a function of snow density (Loth et al., 1993).

2.2.4. Mass balance equations

The snow mass balance equations include the equations for ice and liquid contents. The mass balance of ice content in the snowpack is simplified from Jordan (1991) with the assumption of vapor phase neglected

$$\frac{\partial}{\partial t}(M_{ice}) = U_{ice} - R_{il}\Delta z_{sno} \tag{10}$$

where $U_{ice} = q_{snow} + q_{frost} - q_{sub}$ for the surface layer, and is equal to zero for sub-layers. q_{snow}, q_{frost}, and q_{sub} are snowfall, frost-forming rate and sublimation rate, respectively, which are described in Bonan (1996a). R_{il} is the melting rate (kg m^{-3} s^{-1}).

The mass balance of liquid water for a certain layer of snowpack is

$$\frac{\partial}{\partial t}(M_{liq}) = R_{il}\Delta z_{sno} + (U_{liq}^{in} - U_{liq}^{out}) \tag{11}$$

where $U_{liq}^{in} = q_{rain} + q_{dew} - q_{eva}$ (kg m^{-2} s^{-1}) for the surface snow layer only. q_{rain}, q_{dew} and q_{eva} are rainfall, condensation rate and evaporation rate, respectively. U_{liq}^{out} (kg m^{-2} s^{-1}) is the rate of the excessive liquid water above the holding capacity of the layer flowing down to next layer. U_{liq}^{in} (kg m^{-2} s^{-1}) is the inflowing rate of liquid water from the above layer with a limit of the equivalent water filling the layer pore space within one time step

$$U_{liq}^{in} = \min(U_{liq}^{out}, \phi\rho_{liq}\Delta z_{sno}/\Delta t) \tag{12}$$

where ϕ is the porosity of the sub-layer ($\phi = 1 - \theta_{ice} - \theta_{liq}$), i.e., the available space to store the inflowing water. The excessive water above the saturation becomes runoff. The holding capacity is taken as a function of the layer density following Anderson (1976).

2.2.5. Snow melting and freezing

2.2.5.1. Snow melting. Snow melting occurs only when snow ice exists ($M_{ice} > 0$) and the snow temperature is equal to or above the melting/freezing point ($T_{sno} \geq T_{frz}$) where $T_{frz} = 273.15$ K. In reality, the snow temperature can never be greater than the melting point, so the excessive energy that makes the snow temperature greater than the melting point is used to melt snow ice, and the snow temperature is set back to the melting point ($T_{sno} = T_{frz}$). The melting energy, H_m (W m^{-2}), is given by the following equation

$$H_m = C_{sno} \Delta z_{sno} \frac{T_{sno}^{N+1} - T_{frz}}{\Delta t} \qquad (13)$$

The mass changes $R_{il} \Delta z_{sno}$ (kg m^{-2} s^{-1}) in Eqs. (10) and (11) due to the melting energy H_m can be expressed as

$$R_{il} \Delta z_{sno} = \min(H_m/L_{il}, M_{ice}/\Delta t) \qquad (14)$$

where L_{il} is the latent heat of fusion (0.3336×10^6 J kg^{-1}). If the snow mass M_{ice} in the layer is not enough to be melted by the melting energy H_m, the residual energy is transferred into the next snow or soil sub-layer to conserve energy.

2.2.5.2. Liquid water freezing. Liquid water freezing occurs only if liquid water exists ($M_{liq} > 0$) within snowpack and when snow temperature is below freezing point ($T_{sno} < T_{frz}$). The energy released from freezing is used to increase snow temperature up to the freezing point ($T_{sno} = T_{frz}$) or below freezing point when the liquid water contained in the layer is not sufficient to release energy to make the snow temperature reach the freezing point. Following Loth et al. (1993), the released energy is estimated as

$$H_m = \min(H_{frz}, H_{cold}) \qquad (15)$$

where H_{frz} is the latent energy released from the total liquid water of a layer

$$H_{frz} = M_{liq} L_{il}/\Delta t \qquad (16)$$

and H_{cold} is the cold content of the layer given by

$$H_{cold} = C_{sno} \Delta z_{sno}(T_{frz} - T_{sno}^{N+1'})/\Delta t \qquad (17)$$

where $T_{sno}^{N+1'}$ means the layer temperature resulting from all the processes except for the freezing process. When $H_{frz} < H_{cold}$, i.e., the freezing released energy cannot make up for the cold content, the snow temperature (below freezing point) can be calculated by the following equation,

$$T_{sno}^{N+1} = T_{sno}^{N+1'} + \frac{H_m}{C_{sno} \Delta z_{sno}} \Delta t \qquad (18)$$

$T_{sno}^{N+1} = T_{frz}$, when $H_{frz} > H_{cold}$, according to the above equation. Note that the heat transported by liquid water from the above layer is neglected here.

2.2.6. Densification processes

Following Anderson (1976), the total change in snowpack density or snow depth with time results from three basic processes such as destructive or equi-temperature metamorphism, compaction due to the weight of the overlying snow, and melt metamorphism

$$\frac{1}{\Delta z_{sno}} \frac{\partial \Delta z_{sno}}{\partial t} = CR_1 + CR_2 + CR_3 \qquad (19)$$

where CR_1 is the compaction rate due to destructive metamorphism of new snow, CR_2 is the compaction rate due to the weight of the overlying snow, and CR_3 is the melt metamorphism accounting for the change in snow structure caused by melt–freeze cycles, plus the changes in crystals due to the presence of liquid water. Because the third (or the lowest) layer is rather thick as defined in Eq. (1), CR_2 for this layer also accounts for half of the layer's snow water equivalent (Sun et al., 1999). The melting decreases the depth of the snow cover. All or a portion of the melt water may be retained within the remaining snowpack. Some of this liquid water may in turn refreeze, thereby causing an increase in the ice portion of the snowpack. A melt–freeze cycle will increase the density of the affected portion of the snow cover by several percent.

3. Implementing a topography-based runoff scheme into the NCAR LSM

This section describes a topography-related parameterization of runoff and an implementation of this parameterization into the NCAR LSM. The present parameterization follows closely the TOPMODEL framework (Beven and Kirkby, 1979; Sivapalan et al., 1987) and the recent work of Stieglitz et al. (1997) and Chen and Kumar (2001).

3.1. Saturated hydraulic conductivity

The saturated hydraulic conductivity decreases exponentially with depth according to

$$K_{sat}(z) = K_{sat}(0)e^{-fz} \tag{20}$$

where z is the soil depth (positive downward), $K_{sat}(0)$ is the surface value of saturated hydraulic conductivity, and $1/f$, e-folding depth of K_{sat}, can be determined through sensitivity analysis or calibration against the recession curve of the observed streamflow. According to Chen and Kumar (2001), $K_{sat}(0)$ can be obtained from the compacted value K_s given in Clapp and Hornberger (1978) such that $K_{sat}(0) = K_s e^f$. Such enhancement in the value of $K_{sat}(0)$ by a

factor of e^f is consistent with the surface macropores (Beven, 1982).

In the NCAR LSM, the soil moisture flux is defined at the interface level of the model layers (see Fig. 1):

$$q_{i,i+1} = -k_{i,i+1}\left[\frac{2(\psi_{i+1} - \psi_i) - (\Delta z_i + \Delta z_{i+1})}{\Delta z_i + \Delta z_{i+1}}\right] \tag{21}$$

where i is the layer index, and $q_{i,i+1}$ is the soil moisture flux (positive downward) at the interface level between layers i and $i+1$. ψ_i, Δz_i and ψ_{i+1}, Δz_{i+1} are the matric potential and the layer thickness at layers i and $i+1$, respectively. The hydraulic conductivity at the interface level, $k_{i,i+1}$, is calculated using the thickness-weighted hydraulic conductivities of the surrounding layers,

$$k_{i,i+1} = \frac{k_i k_{i+1}(\Delta z_i + \Delta z_{i+1})}{(\Delta z_i k_{i+1} + \Delta z_{i+1} k_i)} \tag{22}$$

where the symbols are defined in Fig. 1. Recently, several authors have proposed alternative formulations for $k_{i,i+1}$ to improve the accuracy in simulating soil moisture and evaporation (Boone and Wetzel, 1996;
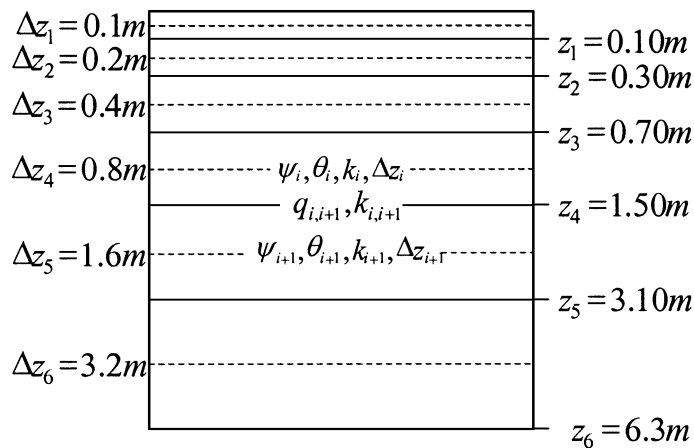

Fig. 1. Schematic diagram of the multilayer soil profile. The hydraulic properties such as volumetric water content θ_i, hydraulic conductivity k_i, and matrix potential ψ_i are defined at the center of a layer with thickness Δz_i, the soil moisture flux $q_{i,i+1}$ and the interfacial hydraulic conductivity $k_{i,i+1}$ are defined between layers.

Dong et al., 2001). In VISA, $k_{i,i+1}$ is parameterized using the arithmetic mean of the volumetric soil moisture content of the surrounding layers θ_i and θ_{i+1},

$$k_{i,i+1} = K_{sat}(z_i)\left[\frac{0.5(\theta_i + \theta_{i+1})}{\theta_{sat}}\right]^{2b+3} \quad (23)$$

where θ_{sat} is the soil porosity, b is a soil parameter depending on soil texture, and $K_{sat}(z_i)$ is the saturated hydraulic conductivity at the soil depth z_i. Different methods of computing the interfacial hydraulic conductivity result in different partial differential equations of $q_{i,i+1}$ with respect to soil moisture. The impacts of using Eq. (22) versus Eq. (23) on runoff will be discussed later.

3.2. Surface runoff

Surface runoff consists of overland flow by the Dunne mechanism which requires rainfall to impinge on a saturated ground surface and overland flow by the Horton mechanism which is generated when rainfall rate exceeds the infiltration capacity of the soil. The mathematical representation of the above processes takes on the form

$$R_s = F_{sat}Q_{wat} + (1 - F_{sat})\max(0, (Q_{wat} - I_{max})) \quad (24)$$

where F_{sat} is the saturated fraction, which is determined by the topographic characteristics and soil moisture state of a grid cell,

$$F_{sat} = \int_{\lambda \geq (\bar{\lambda} + fz_\nabla)} \text{pdf}(\lambda)\,\text{d}\lambda \quad (25)$$

where $\lambda = \ln(a/\tan\beta)$ is the topographic index where a is the contribution area and $\tan\beta$ is the local slope; $\bar{\lambda}$ is the mean value of λ in the grid cell; $\text{pdf}(\lambda)$ is the probability density function of λ; z_∇ is the grid-mean water table depth. Q_{wat} is the recharging rate at the soil surface,

$$Q_{wat} = Q_{melt} + Q_{dew} + Q_{rain} \quad (26)$$

where Q_{melt}, Q_{dew} and Q_{rain} are the water fluxes of snow melting, dew and rainfall.

I_{max} is the soil infiltration capacity dependent on soil texture and moisture conditions (Entekhabi and Eagleson, 1989), which is

$$I_{max} = K_{sat}(0)\left[\left.\frac{\text{d}\psi}{\text{d}z}\right|_{\psi=\psi_{sat}} + 1\right] \quad (27)$$

where ψ_{sat} is the saturated matric potential. The terms inside the bracket represent the gradient of the capillary and gravity forces, respectively, in the vertical direction. The capillary term dominates when the soils are dry. This effect is more pronounced for finer textured soils. When the soils are wet, it can be simplified as $I_{max} = K_{sat}(0)$. Actually, I_{max} for the dryer soil is larger than $K_{sat}(0)$ due to the capillary force. Thus, for TOPMODEL type of runoff scheme, the second term on the right-hand side of Eq. (24), i.e., the Horton runoff, is always zero because of the extremely large $K_{sat}(0)$ due to the surface macropores. However, the infiltration capacity I_{max} is set to zero at the impermeable surfaces such as glaciers, lakes, and wetlands. For the frozen soil surface, I_{max} is parameterized as a function of the partial soil liquid water.

3.3. Subsurface runoff

In the NCAR LSM (Bonan, 1996a), subsurface runoff consists of saturation excess runoff and bottom drainage. In the present approach, the topographic control of subsurface runoff is explicitly included. Subsurface runoff is parameterized as

$$R_{sb} = R_{sb,TOP} + R_{sb,BOT} + R_{sb,SAT} \quad (28)$$

where $R_{sb,TOP}$, $R_{sb,BOT}$, and $R_{sb,SAT}$ represent subsurface runoff due to topographic control, bottom drainage, and saturation excess, respectively.

3.3.1. Topographic control
Following Sivapalan et al. (1987), subsurface runoff due to topographic control is

$$R_{sb,TOP} = \alpha\frac{K_{sat}(0)}{f}e^{-\bar{\lambda}}e^{-fz_\nabla} \quad (29)$$

where α is an anisotropic factor accounting for the differences in the saturated hydraulic conductivities in the lateral and vertical directions introduced by Chen and Kumar (2001) to simulate the desired streamflow response.

3.3.2. Bottom drainage

The gravitational loss of soil water at the bottom of the model soil column is given by

$$R_{sb,BOT} = k_6 + \left(\theta_6^{N+1} - \theta_6^N\right)\left(\frac{\partial k}{\partial \theta}\right)_6 \qquad (30)$$

where k_6 is the hydraulic conductivity at the bottom of the sixth soil layer (Fig. 1), θ_6^N is the volumetric soil moisture within the sixth soil layer at time step N. The bottom drainage depends on f. A large value of f results in a small k_6, and hence a negligible $R_{sb,BOT}$.

3.3.3. Saturation excess

The saturation excess for all soil layers is given in the following equation.

$$W_{excess} = \sum_{i=1}^{6} \max[0, (\theta_i - \theta_{sat})\Delta z_i] \qquad (31)$$

This saturation excess is used to recharge the soil layers above the water table. If the entire column becomes oversaturated, subsurface runoff due to saturation excess is

$$R_{sb,SAT} = \max\left[0, \left(\sum_{i=1}^{6}\theta_i\Delta z_i - \sum_{i=1}^{6}\theta_{sat}\Delta z_i\right)\Big/\Delta t\right] \qquad (32)$$

where Δt is the time step.

3.4. Water table depth

The water table depth z_∇ is crucial in determining the saturated fraction, surface runoff and baseflow. The method of Chen and Kumar (2001) is used here because of its capability to produce a smooth temporal change in water table depth. After the soil moisture is obtained by solving the Richards equation, the soil moisture deficit for the entire column is given by $D_\theta = \sum_{i=1}^{6}(\theta_{sat} - \theta_i)\Delta z_i$. Assuming that there is no vertical moisture flux, then the total head must be conserved within the soil column,

$$\psi(z) - z = \psi_{sat} - z_\nabla \qquad (33)$$

Substituting $\psi(z)$ with the Clapp and Hornberger (1978) formula, we get

$$\psi_{sat}\left(\frac{\theta(z)}{\theta_{sat}}\right)^{-b} - z = \psi_{sat} - z_\nabla \qquad (34)$$

The resulting soil moisture profile is

$$\theta(z) = \theta_{sat}\left(\frac{\psi_{sat} - (z_\nabla - z)}{\psi_{sat}}\right)^{-1/b} \qquad (35)$$

The water table depth, z_∇, is then computed by solving the equality iteratively

$$D_\theta = \int_0^{z_\nabla} (\theta_{sat} - \theta(z))\mathrm{d}z \qquad (36)$$

Computationally, VISA takes the following order. (1) The mean soil moisture is calculated by solving the Richards equation with the infiltration and the bottom drainage as the upper and the lower boundary conditions, respectively. (2) The water table depth is then computed according to the above methodology. (3) The probability density function (pdf) and the water table depth are then used to generate the saturated fraction of a grid cell, that is the area under the cumulative distribution function (CDF) with values of the topographic index greater than $\bar{\lambda} + f z_\nabla$. (4) The saturated fraction determines the fraction of throughfall and snowmelt that becomes surface runoff and infiltration. Subsurface runoff is computed. (5) The evaporative fluxes consist of demand-limited evapotranspiration from the saturated fraction of a grid cell and supply-limited evapotranspiration from the unsaturated fraction.

4. Incorporating a vegetation growth scheme into the NCAR LSM

In terms of the feedback mechanisms represented, the representation of the vegetation in land surface models has evolved through three main phases. First-generation models allowed no feedback between the vegetation and climate and prescribed the vegetation's stomatal resistance as being con-

stant or zero (e.g., Manabe, 1969; Hansen et al., 1983). Second-generation models allowed the vegetation to play a substantial role in determining land surface/atmosphere exchanges, with feedback possible via the parameterization of stomatal resistance/conductance. Based on the work of Jarvis (1976), in such models stomatal conductance depends on the modeled radiation, air temperature, and soil moisture (itself dependent on precipitation), among other things (Dickinson et al., 1993; Sellers et al., 1986). Several authors (e.g., Sellers et al., 1996; Bonan, 1996a; Dickinson et al., 1998) further improved the parameterization of the stomatal conductance by relating it to photosynthesis and carbon assimilation, based on the work of Ball et al. (1987) and Collatz et al. (1991, 1992). While still retaining the conductance–assimilation approach, third-generation models now permit greater feedback between the vegetation and atmosphere. Several important morphological parameters are expressed as a function of precipitation, radiation, temperature, as well as nutrients, such as leaf area index (LAI) (Dickinson et al., 1998), fractional vegetation cover (Huntingford et al., 2000), and competition/distribution (Foley et al., 1998).

In this section, we incorporate the leaf area index growth model of Dickinson et al. (1998) into the NCAR LSM. The leaf growth model of Dickinson et al. (1998) has two major parts: a stomatal conductance–photosynthesis part, and a dynamic leaf part. The first part, similar to the NCAR LSM, is based on Collatz et al. (1991) with photosynthesis being calculated for both sunlit and shaded leaves. The second part is concerned with the changes in carbon allocation, respiration, and vegetation phenology (e.g., budburst, leaf-out, senescence, dormancy). This part resolves time scales from seconds to hours as well as from days to months. Assimilated carbon is allocated to other parts of the plant in addition to the leaves, while the death and decay of leaves and other plant parts release CO_2 back to the atmosphere. The total ecosystem respiration is the sum of four contributions corresponding to maintenance respiration for leaves, wood, roots, and soil, and three contributions corresponding to growth respiration for leaves, wood, and roots. In each case, the maintenance respiration is assumed to be a function of temper-

ature, specifically canopy temperature for leaves and wood respiration, and soil temperatures for root respiration and soil respiration. In each case, growth respiration is assumed to be a specified fraction of the instantaneous carbon assimilation.

When incorporating the leaf growth model of Dickinson et al. (1998) into the NCAR LSM, we only couple the second part of the leaf growth model described above and continue to use the original conductance–photosynthesis model by Bonan (1996a).

5. Model demonstration

This section presents results which demonstrate the capability of VISA in simulating snow, runoff and leaf growth. The Sleepers River watershed is chosen because it provides both snow and runoff measurements. The Boreal Ecosystem-Atmosphere Study (BOREAS) data are used to validate the surface albedo in the presence of snow. The Champaign data set is invaluable to evaluate the predicted leaf area index. Additional demonstration is given by Bowling et al. (2003-this issue) who have documented the performance of VISA in the simulations of snow and runoff for the 58,000-km^2 Torne and Kalix river basins in northern Scandinavia, and in paper 2 which has examined the impacts of different topography-based runoff schemes in VISA.

5.1. Sleepers River watershed

Subcatchment W-3 (8.4 km^2) of the Sleepers River watershed (111 km^2), located in the highlands of Vermont, USA, provides 5 years of meteorological and hydrological data taken between 1969 and 1974 which were used here to drive and evaluate our land surface models. The W-3 topography is characterized by rolling hills and the soils are dominated by silty loams. The vegetation types are approximately one-third grassland, one-third coniferous forest, and one-third deciduous forest. More details are provided by Lynch-Stieglitz (1994) and Stieglitz et al. (1997).

Fig. 2 compares models' results with site data for the entire five snow seasons. The baseline NCAR LSM significantly underestimates snow depth and
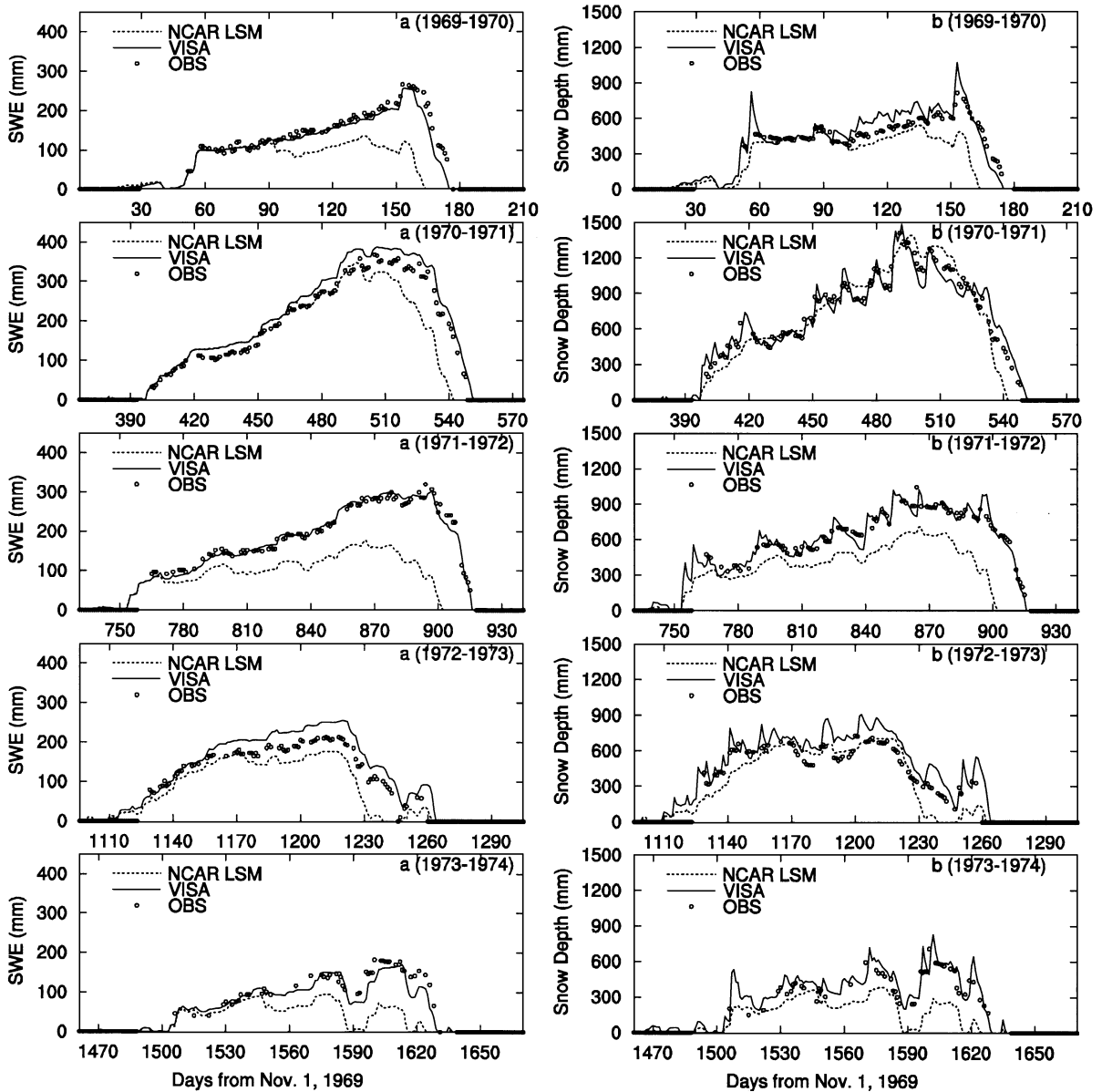
Fig. 2. Modeled snow water equivalent (SWE) and snow depth using the baseline NCAR LSM (dash line) and VISA (solid line) in comparison with observations (squares) for 5 years from November 1, 1969, Sleepers River, USA.

snow water equivalent (SWE). As a result, the timing of the end of the spring snow melt simulated occurs 1–2 weeks too early compared to the observed. These discrepancies are, however, eliminated in the simulations by VISA, which captures the growth and ablation of the snowpack for all snow seasons mainly due

to the inclusion of a thinner snow surface layer and a realistic consideration of water retention and densification processes.

The impacts of using Eq. (23) to represent the hydraulic conductivity at the interface level of model soil layers are illustrated in Fig. 3a. The
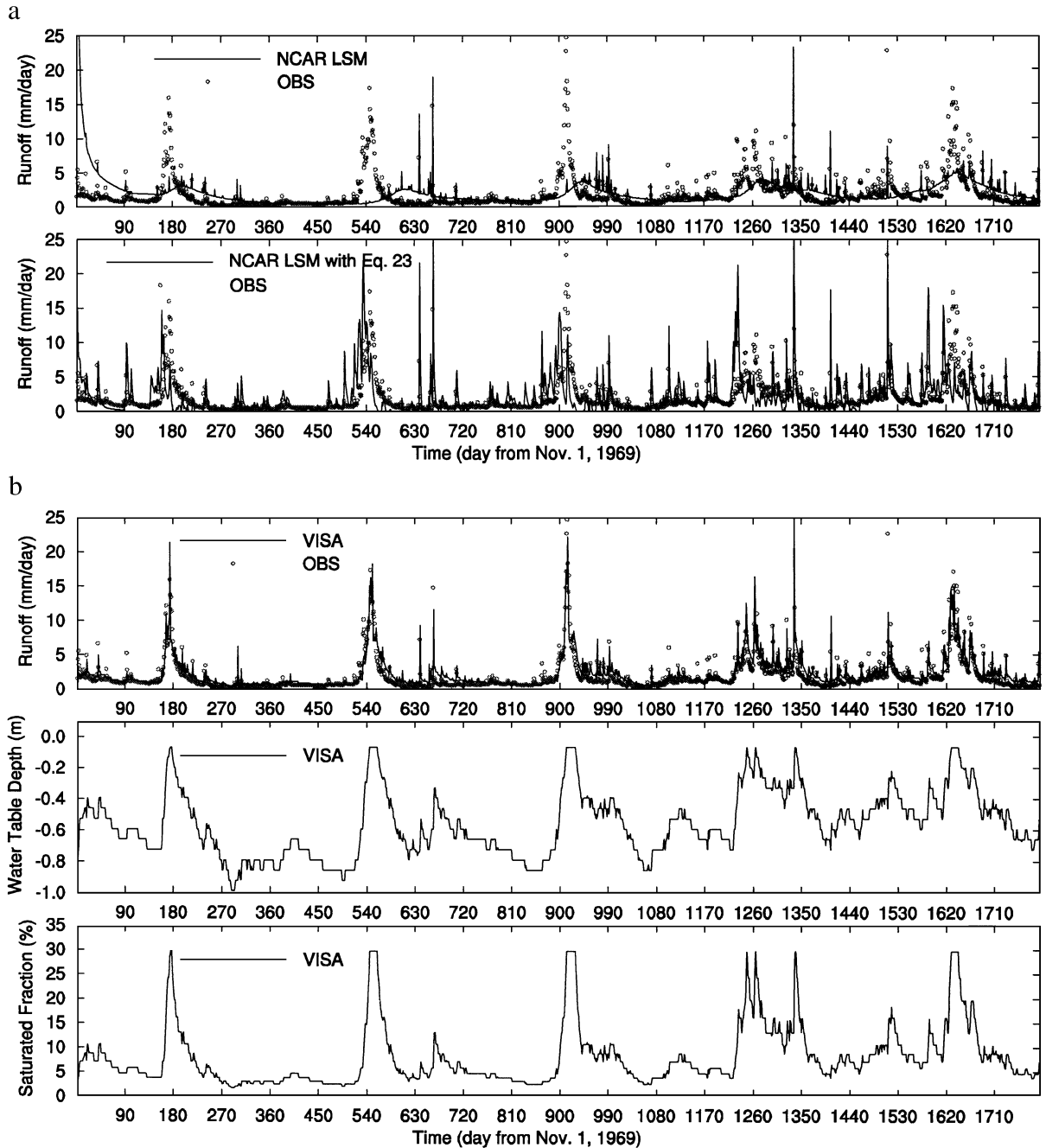
Fig. 3. (a) Modeled daily runoff and observed runoff measured at the W-3 weir. (Top) The baseline NCAR LSM and (bottom) the baseline NCAR LSM with the interfacial soil hydraulic conductivity computed using Eq. (23). (b) (Top) Modeled daily runoff and observed runoff measured at the W-3 weir, (middle) the modeled water table, and (bottom) the modeled saturated fraction.

original formula (cf. Eq. (22)) results in modeled runoff out of phase with observations by up to 3 months. With Eq. (23) used in VISA, the timing and strength of the peak runoff is more accurately simulated, indicating that this new formulation improves the simulations of surface runoff which are generated due to snowmelt, precipitation, or throughfall. However, deficiencies are evident in simulating the slow recession toward nominal values (subsurface runoff) (Fig. 3a). These deficiencies disappear when the TOPMODEL equations are included in VISA (Fig. 3b) in which the hydraulic conductivity decay parameter for the W-3 subcatchment was taken to be 3.26 as given by Stieglitz et al. (1997). As the snowpack ablates in late spring, the water table rises and the saturated fraction increases. As a result, VISA reproduces both the main spring hydrographs and individual storm hydrographs.

5.2. BOREAS data set

VISA also is evaluated with data collected in the boreal forest from the Boreal Ecosystem-Atmosphere Study (BOREAS) (Sellers et al., 1997). Two boreal forest stands located in Southern Study Area (SSA) are selected: mature (old) jack pine (OJP) and old aspen (OA). The focus here is the surface albedo because it is a difficult variable to be properly modeled (Betts and Ball, 1997). Fig. 4 shows that VISA captures the daily variability of surface albedo provided that the observed LAI is used and that the canopy interception capacity for snow is made greater than that for rain. In SSA-OJP, VISA simulates the surface albedo at about 10% during summertime, 15% when snow exists under the canopy, and above 20% during snowfall events. VISA also reproduces the surface albedo in the case of SSA-OA.

5.3. Data at a farmland in Champaign, IL

The data were collected at a farmland in Champaign, IL (40.01°N, 88.37°W). Corn and soybean were planted in alternative years since 1986. Fig. 5 shows that the model not only captures the dynamics of LAI, but also reproduces CO_2 flux, net radiation, latent and sensible heat fluxes, ground heat flux as well as surface temperature and soil moisture at 5-cm depth for both the 1998 soybean
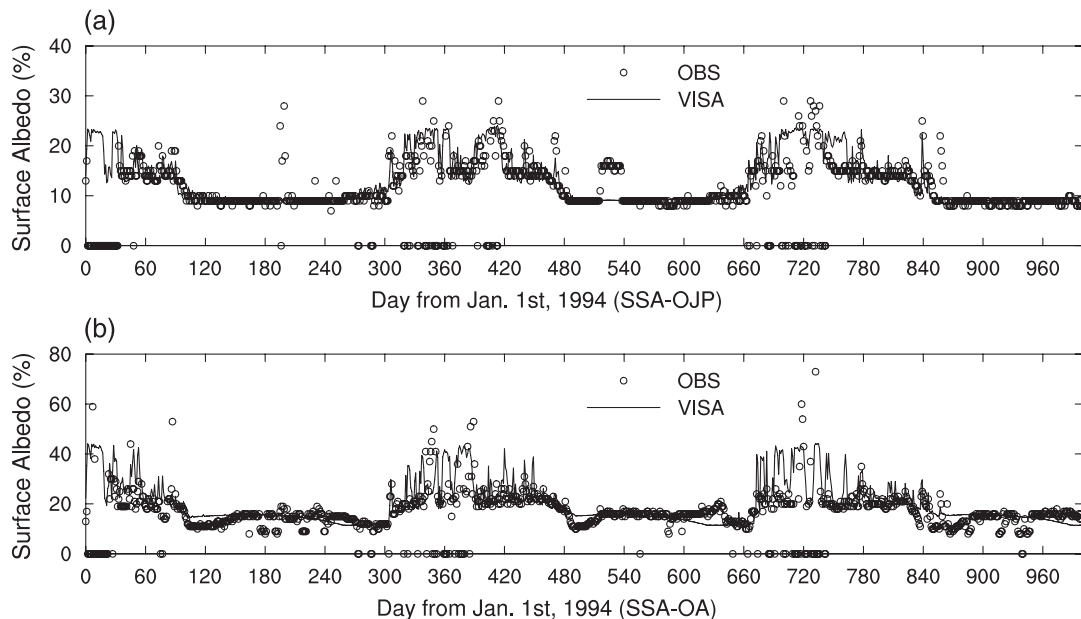

Fig. 4. Comparison of simulated and observed daily mean surface albedo at (a) SSA-OJP, 1994–1996 and (b) SSA-OA, 1994–1996.
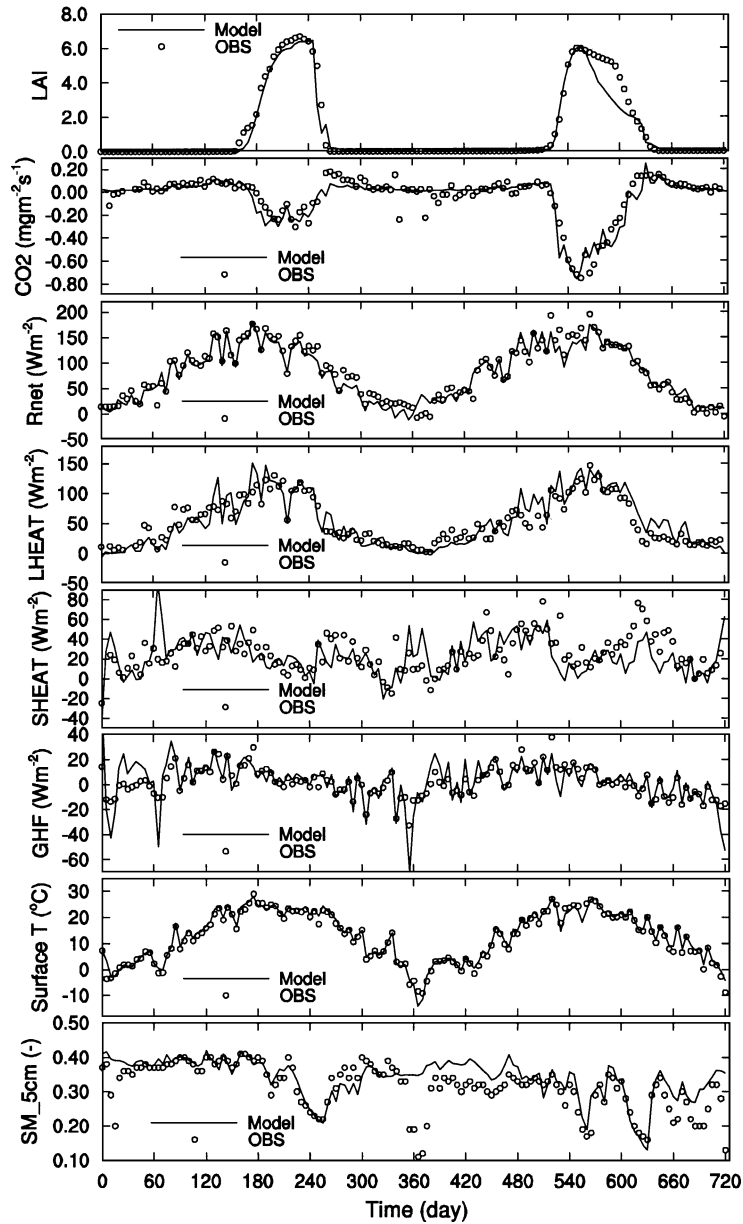
Fig. 5. Modeled 5-day mean leaf area index (LAI), CO_2 flux (CO2), net radiation (Rnet), latent heat flux (LHEAT), sensible heat flux (SHEAT), ground heat flux (GHF), surface temperature and soil moisture at 5 cm (SM_5 cm) in comparison with observations for the 1998 soybean and the 1999 corn.

and the 1999 corn. In addition, the model simulates the diurnal cycle of net radiation, latent and sensible heat fluxes and CO_2 flux (Fig. 6).

The original leaf growth model does not have a stem mass balance equation, thereby leading to excessive allocation of carbon to leaves, much
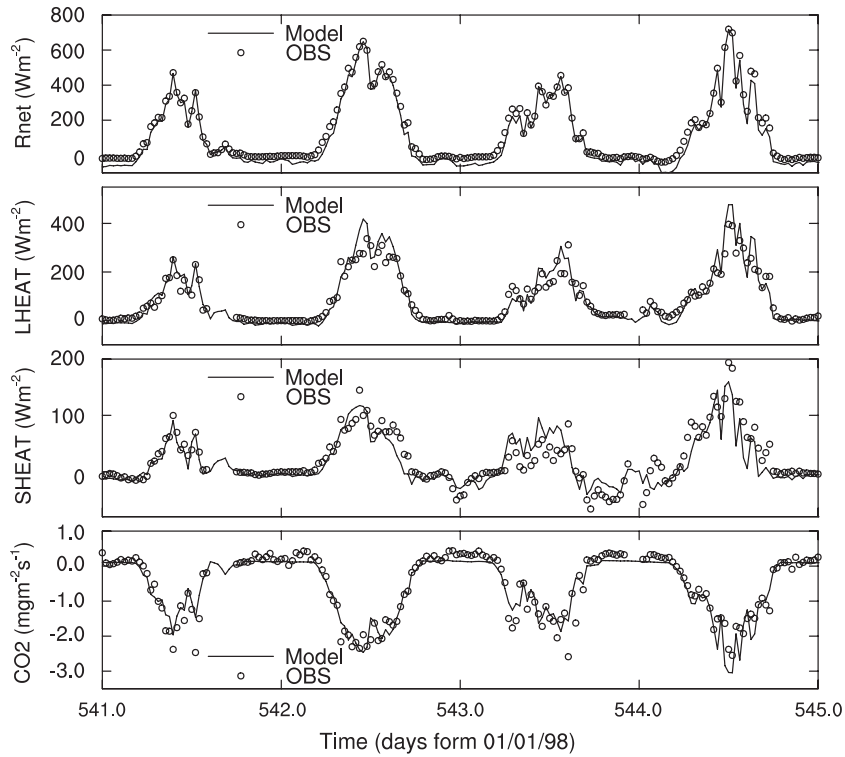
Fig. 6. Diurnal variations of simulated net radiation (Rnet), latent heat flux (LHEAT), sensible heat flux (SHEAT) and CO_2 flux (CO_2) compared with observations for the 4 days selected from the growing season of the 1999 corn.

higher LAI and more uptake of CO_2 in the 1999 corn case. Allowing allocation of the excessive carbon to stem improves the LAI simulations, and the additional stem respiration (upward CO_2 flux) helps improve the simulation of the total CO_2 flux (Fig. 7).
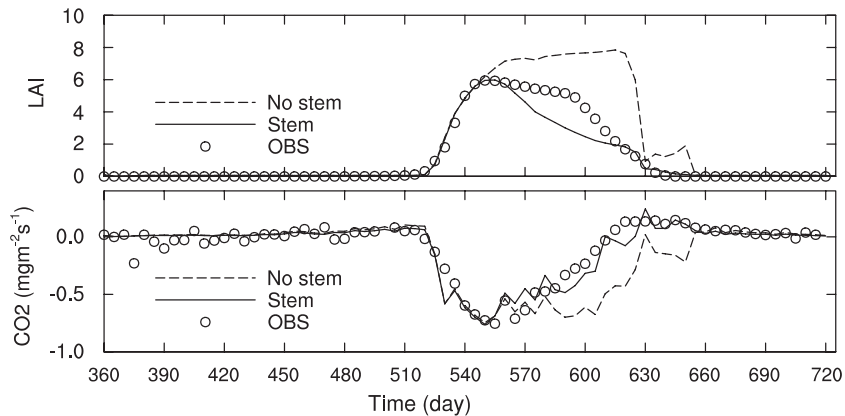

Fig. 7. Modeled leaf area index and CO_2 flux with stem (CTRL) and without stem (no stem) dynamics in comparison with observations for the 1999 corn.

6. Summary

This paper describes three new features that have been added to the baseline version of the NCAR LSM. These new features are (1) a physically based multilayer snow scheme, (2) a topography-based runoff scheme, and (3) a leaf growth scheme. The resulting model is named as the Versatile Integrator of Surface and Atmosphere processes (VISA). VISA has been tested with the Sleepers River data set for both snow and runoff, the BOREAS data set for the surface albedo in the presence of snow, and the Champaign data set for leaf growth.

The baseline NCAR LSM underestimates snow mass and ablates snow too early, which exasperates the problem in simulating snowmelt-induced runoff such that modeled runoff has a weakened amplitude and is several months out of phase with observations. The biases in the snow simulations can be resolved by using the multilayer snow scheme mainly due to the inclusion of a thinner snow surface layer and a realistic consideration of water retention and densification processes. The deficiencies in the timing and strength of runoff are largely due to the method used in computing the hydraulic conductivity at the interface level of the model soil layers. The smoothly fast-rising limb to peak discharge and the gradual recession evident in the main spring hydrographs and individual storm hydrographs can be simulated provided that the TOPMODEL equations are included. As a result, VISA produces realistic simulations of both snow and runoff. Moreover, VISA is capable of simulating leaf growth for soybean and corn in our test case. Results from using VISA on continental and global scales will be reported elsewhere.

Acknowledgements

References

Anderson, E.A., 1976. A point energy and mass balance model of a snow cover. Office of Hydrology, National Weather Service, NOAA Tech. Rep. NWS 19. 150 pp.

Ball, J.T., Woodrow, I.E., Berry, J.A., 1987. A model predicting stomatal conductance and its contribution to the control of photosynthesis under different environmental conditions. In: Biggins, J. (Ed.), Process in Photosynthesis Research, vol. 1. Martinus Nijhoff, pp. 221–234.

Betts, A.K., Ball, J.H., 1997. Albedo over boreal forest. J. Geophys. Res. 102, 28901–28909.

Beven, K.J., 1982. Macropores and water flow in soils. Water Resour. Res. 18, 1311–1325.

Beven, K.J., Kirkby, M.J., 1979. A physically based, variable contributing model of basin hydrology. Hydrol. Sci. Bull. 24, 43–69.

Bonan, G.B., 1995a. Land–atmosphere CO_2 exchange simulated by a land surface process model coupled to an atmospheric general circulation model. J. Geophys. Res. 100, 2817–2831.

Bonan, G.B., 1995b. Sensitivity of a GCM simulation to inclusion of inland water surfaces. J. Clim. 8, 2691–2704.

Bonan, G.B., 1996a. A land surface model (LSM version 1.0) for ecological, hydrological, and atmospheric studies: technical description and user's guide. NCAR Technical Note NCAR/TN-417 + STR. National Center for Atmospheric Research, Boulder, CO. 150 pp.

Bonan, G.B., 1996b. Sensitivity of a GCM simulation to subgrid infiltration and surface runoff. Clim. Dyn. 12, 279–285.

Bonan, G.B., Stillwell-Soller, L.M., 1998. Soil water and the persistence of flood and droughts in the Mississippi River Basin. Water Resour. Res. 34 (10), 2693–2701.

Bonan, G.B., Baldocchi, D., Fitzjarrald, D., Newmann, H., 1997. Comparison of the NCAR LSM1 land surface model with BOREAS aspen and jack pine tower fluxes. J. Geophys. Res. 102 (D24), 19065–29075.

Bonan, G.B., Oleson, K.W., Vertenstein, M., Levis, S., Zeng, X., Dai, Y., Dickinson, R.E., Yang, Z.-L., 2002. The land surface climatology of the Community Land Model coupled to the NCAR Community Climate Model. J. Clim. 15, 3123–3149.

Boone, A., Wetzel, P.J., 1996. Issues related to low resolution modeling of soil moisture: experience with the PLACE model. Glob. Planet. Change 13, 161–181.

Bowling, L.C., Lettenmaier, D.P., Nijssen, B., Graham, L.P., Clark, D.B., Maayar, M.E., Essery, R., Goers, S., Gusev, Y.M., Habets, F., Hurk, B.v.d., Jin, J., Kahanl, D., Lohmann, D., Ma, X., Mahanamao, S., Mocko, D., Nasonova, O., Niu, G.-Y., Samuelsson, P., Shmakin, A.B., Takata, K., Verseghy, D., Viterbo, P., Xia, Y., Xue, Y., Yang, Z.-L., 2003. Simulation of high latitude hydrological processes in the Torne–Kalix basin: PILPS Phase 2(e): 1. Experiment description and summary intercomparisons. Glob. Planet. Change 38, 1–30.

Chen, J., Kumar, P., 2001. Topographic influence on the seasonal and inter-annual variation of water and energy balance of basins in North America. J. Clim. 14, 1989–2014.

Clapp, R.B., Hornberger, G.M., 1978. Empirical equations for some soil hydraulic properties. Water Resour. Res. 14, 601–604.

Collatz, G.J., Ball, J.T., Grivet, C., Berry, J.A., 1991. Physiological

and environmental regulation of stomatal conductance, photosynthesis and transpiration—a model that includes a laminar boundary layer. Agric. For. Meteorol. 54 (2–4), 107–136.

Collatz, G.J., Ribascarbo, M., Berry, J.A., 1992. A coupled photosynthesis–stomatal conductance model for leaves of C_4 plants. Aust. J. Plant Physiol. 19, 519–538.

Dai, Y.-J., Zeng, Q.-C., 1997. A land surface model (IAP94) for climate studies: I. Formulation and validation in off-line experiments. Adv. Atmos. Sci. 14, 433–460.

Dai, Y., Zeng, X., Dickinson, R.E., Baker, I., Bonan, G., Bosilovich, M., Denning, S., Dirmeyer, P., Houser, P., Niu, G.-Y., Oleson, K., Schlosser, A., Yang, Z.-L., 2003. The Common Land Model (CLM). Bull. Am. Meteorol. Soc. (in press).

Dickinson, R.E., Henderson-Sellers, A., Kennedy, P.J., 1993. Biosphere–Atmosphere Transfer Scheme (BATS) version 1e as coupled to the NCAR Community Climate Model. NCAR Technical Note NCAR/TN-387 + STR, Boulder, CO. 72 pp.

Dickinson, R.E., Shaikh, M., Bryant, R., Graumlich, L., 1998. Interactive canopies for a climate model. J. Clim. 11, 2823–2836.

Dong, J., Salvucci, G.D., Myneni, R.B., 2001. Improving the precision of simulated hydrologic fluxes in land surface models. J. Geophys. Res. 106 (D13), 14357–14368.

Entekhabi, D., Eagleson, P.S., 1989. Land surface hydrology parameterization for atmospheric general circulation models including subgrid-scale spatial variability. J. Clim. 2, 816–831.

Famiglietti, J.S., Wood, E.F., Sivapalan, M., Thongs, D.J., 1992. A catchment scale water balance model for FIFE. J. Geophys. Res. 97, 18997–19007.

Foley, J.A., Levis, S., Prentice, I.C., Pollard, D., Thompson, S.L., 1998. Coupling dynamic models of climate and vegetation. Glob. Chang. Biol. 4, 561–579.

Hansen, J., Russell, G., Rind, D., Stone, P., Lacis, A., Lebedeff, S., Ruedy, R., Travis, L., 1983. Efficient three-dimensional global models for climate studies: models I and II. Mon. Weather Rev. 3 (4), 609–662.

Huntingford, C., Cox, P.M., Lenton, T.M., 2000. Contrasting responses of a simple terrestrial ecosystem model to global change. Ecol. Model. 134 (1), 41–58.

Jarvis, P.G., 1976. The interpretation of the variations in leaf water potential and stomatal conductance found in canopies in the field. Philos. Trans. R. Soc. Lond., B 273, 593–610.

Jordan, R., 1991. A one-dimensional temperature model for a snow cover. U.S. Army Corps of Engineers, Cold Regions Research and Engineering Laboratory (Special Report 91-16).

Kiehl, J.T., Hack, J.J., Bonan, G.B., Boville, B.A., Williamson, D.L., Rasch, P.J., 1998. The National Center for Atmospheric Research Community Climate Model: CCM3. J. Clim. 11, 1131–1149.

Loth, B., Graf, H.-F., Oberhuber, J.M., 1993. Snow cover model for global climate simulations. J. Geophys. Res. 98, 10451–10464.

Lynch-Stieglitz, M., 1994. The development and validation of a simple snow model for the GISS GCM. J. Clim. 7, 1842–1855.

Manabe, S., 1969. Climate and the ocean circulation: 1. The atmospheric circulation and the hydrology of the Earth's surface. Mon. Weather Rev. 97, 739–774.

Niu, G.-Y., Yang, Z.-L., 2003a. A physically based multi-layer snow parameterization for the NCAR CCM3/LSM: Part I. Validation and sensitivity tests in stand-alone experiments. J. Clim. (submitted for publication).

Niu, G.-Y., Yang, Z.-L., 2003b. The Versatile Integrator of Surface Atmospheric Processes (VISA): Part 2. Evaluation of three topography-based runoff schemes. Glob. Planet. Change 38, 191–208.

Sellers, P.J., Mintz, Y., Sud, Y.C., Dalchier, A., 1986. A Simple Biosphere model (SiB) for use within General Circulation Models. J. Atmos. Sci. 43, 505–531.

Sellers, P.J., Randall, D.A., Collatz, G.J., Berry, J.A., Field, C.B., Dazlich, D.A., Zhang, C., Collelo, G.D., Bounoua, L., 1996. A revised land surface parameterization (SiB2) for atmospheric GCMs: Part I. Model formulation. J. Clim. 9, 676–705.

Sellers, P.J., Hall, F.G., Kelly, R.D., Black, A., Baldocchi, D., Berry, J., Ryan, M., Ranson, K.J., Crill, P.M., Lettenmaier, D.P., Margolis, H., Cihlar, J., Newcomer, J., Fitzjarrald, D., Jarvis, P.G., Gower, S.T., Halliwell, D., Williams, D., Goodison, B., Wickland, D.E., Guertin, F.E., 1997. BOREAS in 1997: experiment overview, scientific results, and further directions. J. Geophys. Res. 102 (D24), 28731–28769.

Sivapalan, M., Beven, K., Wood, E.F., 1987. On hydrologic similarity: 2. A scaled model of storm runoff production. Water Resour. Res. 23, 2266–2278.

Stieglitz, M., Rind, D., Famiglietti, J., Rosenzweig, C., 1997. An efficient approach to modeling the topographic control of surface hydrology for regional and global modeling. J. Clim. 10, 118–137.

Sun, S.F., Jin, J.M., Xue, Y., 1999. A simple Snow–Atmosphere–Soil Transfer (SAST) Model. J. Geophys. Res. 104, 19587–19597.

Yang, Z.-L., Niu, G.Y., 2000. Snow–climate interaction in NCAR CCM3. Preprints, 15th Conference on Hydrology, American Meteorological Society Meeting, Long Beach, California, USA, January 2000, pp. 24–27.

Zeng, X., Shaikh, M., Dai, Y., Dickinson, R.E., Myneni, R., 2002. Coupling of the Common Land Model to the NCAR Community Climate Model. J. Clim. 15, 1832–1854.